PHYSICAL REVIEW B VOLUME 47, NUMBER 4 15 JANUARY 1993-II

Temperature dependence of interlayer spacings and mean vibrational amplitudes at the Al(110) surface

H. Göbel and P. von Blanckenhagen
Kernforschungszentrum Karlsruhe, Institut für Materialforschung I, P.O. Box 3640, W-7500 Karlsruhe, Germany
(Received 23 July 1992; revised manuscript received 25 September 1992)

The Al(110) surface has been studied by low-energy electron diffraction experiments performed in the temperature range from 40 to 890 K. The three outermost interlayer spacings, the inner potential, and the rms-vibrational amplitudes normal to the surface were determined between 40 and 450 K by a kinematical analysis of the $I(E)$ spectra. In this temperature range a negative expansion coefficient for the first interlayer spacing and a temperature-dependent inner potential was found. At higher temperatures the mean thermal expansion coefficient was derived by the peak-shift method, taking into consideration the Debye-Waller factor and the inner potential. A strongly enhanced linear thermal expansion coefficient was observed above 750 K.

I. INTRODUCTION

The temperature dependence of the structure and dynamics at solid surfaces depends mainly on the temperature dependence of the surface free energy and on the anharmonicity of the interatomic interactions at the surface. Phenomena such as lattice relaxation, roughening, and premelting, as well as the enhancement of thermal expansion and of mean thermal vibrational amplitudes in comparison to the bulk values, are of fundamental interest. In order to elucidate these phenomena and to develop and test microscopic models for surfaces, detailed experimental studies of the structure and dynamics in wide temperature ranges up to the melting point are needed. Recently, the temperature dependence of structures of some surfaces has been investigated by molecular-dynamics (MD) simulations by which the anharmonicity of the applied interatomic interaction is fully considered.

The multilayer relaxation at the Al(110) surface has previously been studied extensively at two different temperatures in low-energy electron diffraction (LEED) experiments, combined with intensity calculations made within the framework of the dynamical scattering theory.[1,2] It has been possible to calculate in model calculations the multilayer relaxation for $T = 0$ (see Table I), but no theoretical data are as yet available for the temperature dependence of the outermost interlayer spacings. The premelting effect at this surface was first detected in LEED experiments[3] and studied in detail in medium energy ion scattering (MEIS) experiments[4,5] and by MD calculations.[6–8]

The thermal expansion at several other surfaces was already studied by LEED [Xe(111),[9] Kr(111),[10] W(001),[11] Ni(001) (Ref. 12)] and MEIS [Pb(110) (Ref. 13)] experiments as well as by model calculations [Kr(111),[10] Cu(110),[14] Ni(110) (Ref. 15)]. Strong enhancements of the thermal expansion normal to the surface in comparison to the thermal expansion in the bulk were found in these cases, at least at high temperatures.

We performed LEED experiments between 40 and 890 K. By kinematical analysis of the $I(E)$ spectra taken in the low-temperature range (40–450 K) it was possible to determine the first three interlayer spacings as well as the mean vibrational amplitudes normal to the surface in the first two outermost layers as well as in the bulk. The method used in this data analysis is equivalent to the method applied recently in the analysis of surface x-ray diffraction data for other surfaces.[16]

At higher temperatures we use the well-established peak-shift method[12,17] by which a mean thermal expansion coefficient averaged over the penetration depth of the electrons could be derived.

This paper is organized as follows. In Sec. II the experimental conditions and in Sec. III the methods used for the data analysis will be described; the results will be presented in Sec. IV and discussed in Sec. V.

II. EXPERIMENT

The experiments were performed in a UHV chamber equipped with a reverse-view LEED system, Auger electron spectroscopy (AES) system, 2-kV sputter gun, and quadrupole mass analyzer. The base pressure in the chamber is $\approx 5 \times 10^{-11}$ mbar. The surface of the commercial Al crystal (10 mm diam, 99.999% purity) is cut parallel to the (110) surface with an accuracy of 0.15°. The surface is cleaned by alternating Ar^+ sputtering and annealing at 800 K until no more contamination is detectable by AES spectroscopy (O contamination $\leq$ 0.01 ML). The diffracted intensity is measured with a video-LEED system. The LEED optics is a conventional three-grid optics which allows partial separation of the inelastic background. The $I(E)$ spectra of the specular spot are measured by direct integration of the intensity contained in a window around the spot position.

The data presented in the next section are collected from several independent runs under variation of the sample temperature starting with a freshly prepared sur-

face in each case. The temperature was stabilized within ±1 K.

III. METHODS OF DATA ANALYSIS

A. Peak-shift analysis

The Bragg condition for a specular reflex is given by

$$E_B = E_P + V_i = \frac{150.4}{4d_\perp^2 \cos^2\theta} n^2, \tag{1}$$

where E_P (eV) is the expected position of a Bragg peak in the $I(E)$ spectra, V_i (eV) is the inner potential, θ is the incident angle with respect to the normal of the surface, $d_\perp$ (nm) is the interlayer spacing, and n is the diffraction order. The mean linear thermal expansion coefficient averaged for the first interlayer spacings as determined by the mean free path of the electrons defined by

$$\alpha = \frac{1}{d_\perp}\frac{\partial d_\perp}{\partial T}$$

can be derived with Eq. (1) as

$$\alpha = -\frac{1}{2}\frac{\partial \ln E_B}{\partial T} = -\frac{1}{2}\frac{\partial \ln(E_P + V_i)}{\partial T}. \tag{2}$$

The applicability of this peak-shift method was clearly demonstrated by Cao and Conrad[12] and Webb and Lagally.[17] In general, the inner potential has to be considered at least for low- and medium-energy electrons. In the determination of E_P as a function of the temperature the influence of the Debye-Waller factor on E_P has to be considered, too, because this effect would reduce the value of α [Eq. (2)] by the term

$$\frac{1}{E_P^2}\frac{\partial \ln I/I_0}{\partial T}\frac{\sigma^2}{16\ln 2}, \tag{3}$$

which is equivalent within the Debye approximation[18] to the following term:

$$\frac{1}{E_P^2}\frac{Q_\perp^2\langle u_\perp^2\rangle}{T}\frac{\sigma^2}{16\ln 2} \tag{4}$$

with $\sqrt{\langle u_\perp^2\rangle}$ the rms vibrational amplitude. The refinement of the peak-shift method by considering both the inner potential and the Debye-Waller factor will be demonstrated below.

The data analysis described above is correct if the contribution from multiple scattering to the measured intensity is negligible. Since multiple scattering would depend on the incidence and azimuth angles, a kinematical analysis of the data is justified if α is independent of these angles. Such a proof was already successfully applied in an earlier work by Cao and Conrad.[12]

B. Kinematical calculation of $I(E)$ spectra and parameter determination

Instead of the dynamical theory we use the kinematical diffraction theory for data analysis because we intend to show that a kinematic analysis can be made if the experiment is optimized accordingly. An advantage of the kinematical theory is the significantly reduced expenditure in terms of calculation work.

Whereas, on the one hand, no kinematical analysis has been made so far to determine the temperature dependence of interlayer spacings and of mean vibrational amplitudes by LEED experiments, this method, on the other hand, is well established in the study of step density, growth processes, and roughening transitions by LEED experiments.[19–23] In all these cases multiple-scattering effects have been neglected, i.e., they do not affect the information obtained. In our case, the influence of multiple-scattering effects is checked in a peak-shift analysis as described above.

Since the aim of the analysis is the determination of the interlayer spacings, the $I(E)$ spectra of the specular reflex (00) are the most sensitive quantity to be measured.

Within the framework of the kinematical diffraction theory the $I(E)$ spectra for the specular Bragg reflex of a monoatomic lattice is given by the following equation:

$$I(E,\theta) = N_1^2 N_2^2 \left| \sum_{j=1}^{N_\perp} f(E,\theta) \exp\left(iQ_\perp r_{\perp,j}\right) \exp\left(-\frac{2r_{\perp,j}}{\lambda\cos\theta}\right) \exp\left(-\tfrac{1}{2}Q_\perp^2\langle u_{\perp,j}^2\rangle\right) \right|^2, \tag{5}$$

with N_1 and N_2 being the numbers of the atoms in the two main directions of symmetry parallel to the surface, $N_\perp$ the number of atom layers which contribute to the scattering intensity, $Q_\perp$ the perpendicular momentum transfer, $Q_\perp = \frac{\sqrt{8m_e}}{\hbar}\cos(\theta)\sqrt{E+V_i}$, and $r_{\perp,j}$ the position of the layer j perpendicular to the surface. The scattering amplitude $f(E,\theta)$ was calculated from the phase shifts provided by van Hove;[24] it depends strongly on the electron energy between 10 and 100 eV showing the maximum at about 70 eV and a slow and monotonous decrease above 100 eV. $\lambda(E)$ is the electron mean free path,[25] which is responsible for the fact that only a few ($N_\perp$) layers contribute to scattering. The factor of $2r_{\perp,j}/\cos\theta$ is due to the total path of the electron beam inside the crystal. The energy dependence of λ was described in Ref. 25 by the following empirical equation:

$$\lambda(E) = a\left(\frac{538}{E^2} + 0.41\sqrt{aE}\right), \tag{6}$$

derived by adaption to experimental mean free path data, where a (nm) is the monolayer thickness. A theoretical analysis[26] has shown that the attenuation of the electron beam is due mainly to inelastic processes.

In order to study the influence of the angular and energy uncertainties on the peak width, calculations considering Gaussian resolution functions were performed. It appeared that the full width at half maximum of the Bragg peaks in the $I(E)$ spectra are caused mainly by the small penetration depth and the influence of the energy and angle uncertainties can be neglected under the present experimental conditions. The term $\exp(-Q_\perp^2\langle u_{\perp,j}^2\rangle)$ with the rms thermal vibrational amplitude $\sqrt{\langle u_\perp^2\rangle}$ is the Debye-Waller factor.

The interlayer spacings d_{ij} and their relative changes with respect to the bulk values Δd_{ij} are related to $r_{\perp,j}$ as follows:

$$d_{ij} = r_{\perp,j} - r_{\perp,i}, \quad \Delta d_{ij} = \frac{d_{ij} - d_{\text{bulk}}}{d_{\text{bulk}}}.$$

In our calculation we assumed that only the rms-vibrational amplitudes in the first two outermost layers are greater than in the bulk, because results from MEIS experiments [Pb(110) (Ref. 13) and Al(110) (Ref. 4)] were compatible with a 50% enhancement of the rms-vibrational amplitudes in the first and 25% the second layer.

Figure 1 shows a comparison between a calculated [Eq. (5)] spectrum and an experimental $I(E)$ spectrum recorded at 76 K. The parameters for the simulation are taken from the literature.[1,27] Two types of peaks can be clearly recognized in both spectra: the Bragg peaks which appear at the energies E_B, and between them, the broad peaks caused by lattice relaxation. The very good qualitative agreement between both spectra is an indication of the applicability of the kinematical scattering theory to Al(110) LEED data.

For a quantitative comparison of experimental $I^e(E)$ and calculated $I^c(E)$ spectra we applied the following reliability factor:[18]

$$R1 = \frac{\sum_i |I^e(E_i) - I^c(E_i)|}{\sum_i |I^e(E_i)|} \tag{7}$$

because calculations with different R factors showed that we got the best fits, controlled by eye, with the advantage of a short converging time, when we used this $R1$ factor.

To get the best fit we used the so-called GRID-search algorithm[28] in order to find the minimum of $R1$. This algorithm offers the advantage that the procedure of optimisation and the optimum values of the parameters are relatively insensitive to the initial values of the parameters. The following parameters were varied in the fit procedure and their starting values were taken from the literature as indicated below.

Interlayer spacing for the bulk. Temperature-dependent data are extracted from single crystal densities[29] and thermal expansion coefficients.[30] Both data sets show a very good agreement with each other.

Interlayer spacing for the first four layers and the inner potential at T=100 K. The data were taken from the LEED data analysis[1] (see Table I).

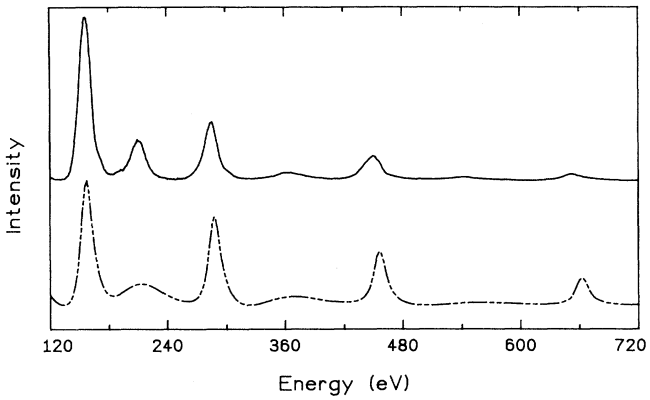

FIG. 1. Comparison between an $I(E)$ spectrum (solid line) measured at $T = 76$ K with $\theta = 7°$ and a kinematically calculated spectrum (dashed line) according to Eq. (5) with relaxation parameters taken from Ref. 1 and bulk vibrational amplitudes from Ref. 27.

rms vibrational amplitude for the bulk and an enhancement of the rms vibrational amplitudes in the first two layers of 50% for the first layer and of 25% for the second layer. The enhancement was chosen on the assumption made for the description of MEIS data.[4,13] The bulk values are calculated from temperature-dependent theoretical data[27] which at 300 K are in good agreement with an average value derived from a number of experimental results.[31]

A background with linear dependence on the electron energy. This background is due to a constant electronic noise as well as to energy-dependent diffuse scattering.

The statistical uncertainties of the optimized parameters are directly evaluated from the last iteration step width of the variables.[28]

For an optimal application of the described method of kinematical data analysis a suitable range of electron energies has to be selected. On the one hand, the energy should be so high that the scattering amplitude is not strongly energy dependent (i.e., greater than 100 eV) and, on the other hand, the energy should not be so high so that the scattered intensity would not be reduced too much by the Debye-Waller factor. For this reason, we have selected a range of electron energies between 130 and 320 eV. For data analysis a constant scattering amplitude was assumed; this is justified because the weak energy dependence of $f(E,\theta)$ in the selected range of energies has a negligible influence on the fitting parameters. This energy dependence of $f(E,\theta)$ would cause an increase in the resulting vibrational amplitudes smaller than their statistical uncertainties since the intensity depends exponentially on the square of the vibrational amplitudes.

The temperature range for which the LEED data are sufficient to make a layer-resolved analysis is limited first by the decreasing peak to background ratio due to the Debye-Waller factor and the inelastic background and second by the influence of the step formation on the $I(E)$ spectra. For Al(110) the roughening transition was found

TABLE I. Comparison of measured and calculated relative interlayer spacings for the Al(110) surface.

Reference		T (K)	Δd_{12} (%)	Δd_{23} (%)	Δd_{34} (%)	Δd_{45} (%)
Barnett *et al.* (Ref. 49)	Theory	0	-10	4	-3	
Ho and Bohnen (Ref. 43)	Theory	0	-6.8	3.5	-2.0	1.6
Chen *et al.* (Ref. 51)	Theory	0	-10.36	3.23	-2.58	1.58
Eguiluz (Ref. 42)	Theory	0	-5.4	1.2	-3.0	
Ning *et al.* (Ref. 50)	Theory	0	-10.47	3.64	-2.93	-1.45
Smith and Baneciea (Ref. 48)	Theory	0	-10.1	4.8	-0.4	
Ditlevsen and Nørskov (Ref. 45)	Theory	0	-6	1		
Anderson *et al.* (Ref. 1)	LEED	100	-8.6	5.0	-1.6	
Noonan and Davis (Ref. 2)	LEED	297	-8.5	5.5	2.2	1.6
Present work	LEED	70	-6.9	4.1	-3.7	
Present work	LEED	316	-7.6	5.0	-3.2	

to appear between 400 and 500 K.[32,33] An introduction of a step parameter into Eq. (5), as demonstrated in Ref. 16, was not successful due to the restricted range of energies. The maximum sample temperature for the analysis has been found to be about 450 K.

The selected range of the incidence angles θ was between 5.5° and 8° because the agreement between the measured and calculated $I(E)$ spectra are best there. At greater incidence angles ($\theta > 12°$) the measured spectra exhibited additional structures which have not been found in the calculated spectra.

IV. RESULTS

A. Peak-shift analysis

Before starting the data analysis according to Eq. (5) it has to be examined whether multiple-scattering effects can be neglected. Figure 2 shows the specular reflex (002) at an energy of about 64 eV for two different temperatures with the same scale of intensities. The peak shift is apparent and, also at 873 K, the peak is definitely separable from the background. A computer program was used to determine the energy of the maxima of the peak under consideration of the background intensity. Such peak profiles were measured at different incidence ($5° \leq \theta \leq 19°$) and azimuth angles ($0° \leq \Phi \leq 70°$). The energy values of the peak maxima are corrected applying a temperature-independent inner potential of 12 eV,[34,35] as described in Eq. (2). In Fig. 3(a) $\ln[E/E(0)]$ is plotted, where $E(0)$ is the peak position at 40 K. The line drawn is a least-squares fit to all data indicating a constant expansion coefficient up to 750 K; a nearly constant value has been expected from literature data for the bulk.[30] Above 750 K the peak shift is strongly en-

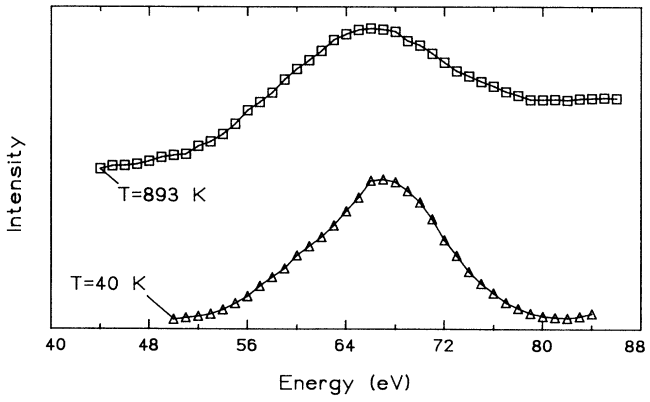

FIG. 2. $I(E)$ spectra for the specular spot around the (002) position for T=40 and 873 K. The incidence angle is $\theta = 9°$.

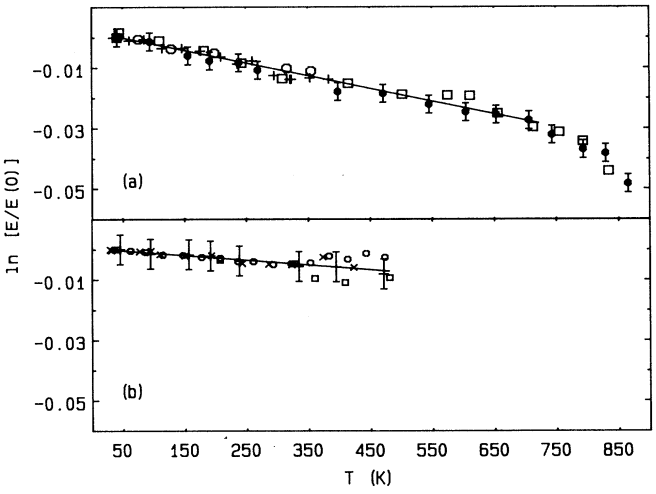

FIG. 3. The logarithm of the peak position (energy shift with respect to the value at 40 K) vs temperature with a fitted straight line. Each symbol corresponds to a measurement with a different incidence or azimuth angle: (a) For an electron energy of 64 eV the symbols denote the following. ○: $\theta = 6.5°$, $\Phi = 0°$; +: $\theta = 5°$, $\Phi = 10°$; •: $\theta = 7°$, $\Phi = 70°$; □: $\theta = 19°$, $\Phi = 0°$. (b) For an electron energy of 285 eV the symbols denote the following. □: $\theta = 6°$, $\Phi = 0°$; ○: $\theta = 5°$, $\Phi = 10°$; +: $\theta = 7°$, $\Phi = 70°$; ×: $\theta = 5.5°$, $\Phi = 0°$.

hanced. The analysis leads to an α value three times greater than the value below 750 K. Figure 3(b) shows the data for the (004) peak at about 285 eV. At this energy the measurement ends at 480 K because, due to the decreased Debye-Waller factor, the intensities of the peaks at higher temperatures were too low compared to the background to allow the peak maxima to be evaluated. The quantitative data analysis for determination of the thermal expansion coefficient derived from the two different Bragg peaks is given at the end of Sec. V, because the temperature dependence of the inner potential, which is needed for the derivation of α, will be discussed later.

The experimental results shown in Fig. 3 indicate that multiple-scattering effects have no significant influence on the peak shift. The deviations of the data obtained by measurements with different angular parameters are within the experimental errors. This result, together with the overall agreement between measured and calculated $I(E)$ spectra depicted in Fig. 1, justifies the application of the kinematical theory according to Eq. (5) in the analysis of the experimental $I(E)$ spectra.

B. Analysis of the $I(E)$ spectra

As discussed in Sec. III, a quantitative analysis of the $I(E)$ spectra is possible only in a restricted range of energies. The results of the fitting procedure for $I(E)$ spectra at 70 and 321 K are shown in Fig. 4 where the experimental data are plotted together with calculated data corresponding to the best fit. The $R1$ factor derived from the data at $T = 70$ K is 0.091 and at $T = 321$ K it is 0.031. These values demonstrate the high quality of the fits implying that the temperature dependence of interlayer spacings, rms vibrational amplitudes, and the inner potential can be determined. The value of the $R1$ factor for all fits are in the range of $0.032 \leq R1 \leq 0.16$. A perspective view of the $R1$ factor as a function of Δd_{12} and Δd_{23} for the data at $T = 70$ K is shown as an example in Fig. 5. This plot demonstrates that a well-defined minimum exists of the $R1$ factor as a function of the parameters Δd_{12} and Δd_{23}. Whereas these two parameters were varied, the other parameters were maintained at their optimized values. The smallest $R1$ factor of 0.091 is found for $\Delta d_{12} = -6.88\%$ and $\Delta d_{23} = 4.11\%$.

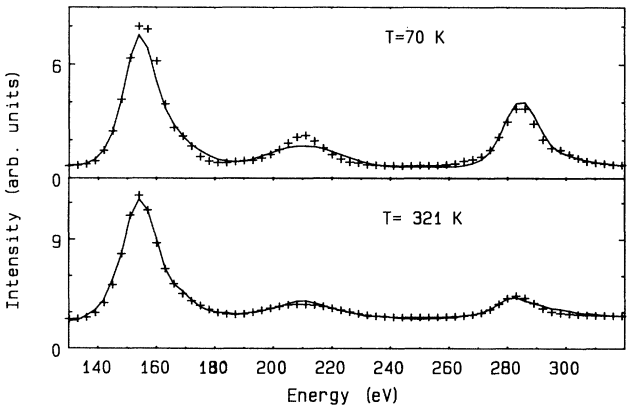

FIG. 4. Intensity vs energy $I(E)$ spectra for two different temperatures. + are the experimental data and the line represents the best fit with calculated data according to Eq. (5). Angle of incidence is $\theta = 8°$. The value of $R1$ is 0.091 at $T = 70$ K and 0.031 at $T = 321$ K, respectively.

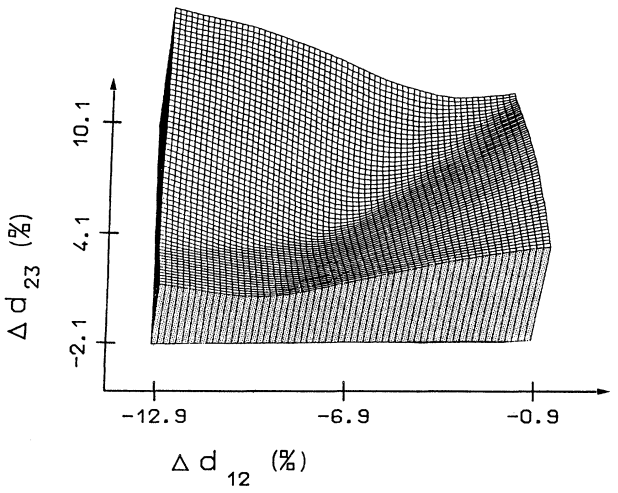

FIG. 5. Perspective view of the $R1$ factor as a function of Δd_{12} and Δd_{23}, constructed for fixed, optimum values of the other parameters derived from an $I(E)$ spectra at 70 K.

1. *Temperature dependence of the multilayer relaxation*

A series of $I(E)$ spectra were measured and analyzed for a temperature range from 40 to 420 K. For $I(E)$ spectra at higher temperatures the peak to background ratio is too small due to a small Debye-Waller factor and due to high thermal diffuse scattering so that it is impossible to get a good fit. In Fig. 6 the results of the fits are shown

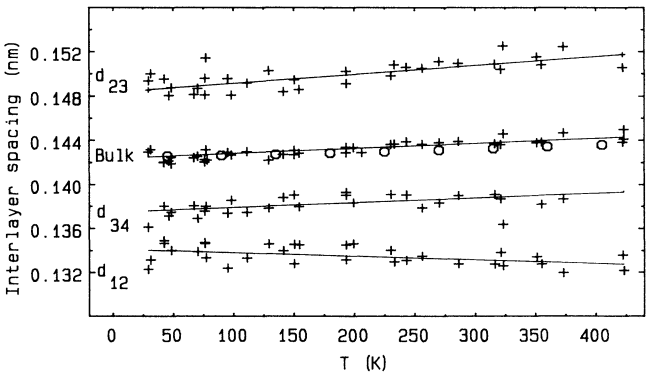

FIG. 6. Temperature dependence of the interlayer spacings at the surface and in the bulk. The straight lines are results of a fit to the data representing the thermal expansion. ○ are the bulk interlayer spacings taken from Ref. 30.

for the first three and the bulk interlayer spacings. The data for each interlayer spacing were fitted with a straight line in order to derive the linear thermal expansion coefficient and to visualize the temperature dependence of the data. For comparison of the results for the bulk interlayer spacing with data from the literature, the bulk values from Hatch[30] are also plotted in Fig. 6 (open circles). There is good agreement between our results and the literature data for thermal expansion.

The contracted first interlayer spacing at the surface decreases with increasing temperature. The results yield a contraction with a coefficient of -24×10^{-6} K^{-1} for the first interlayer spacing with a statistical error of about 10%. Analyzing the expanded second interlayer spacing d_{23} we obtained a thermal expansion coefficient which is about two times greater than the bulk value from literature,[30] which is 24×10^{-6} K^{-1}. The contracted third interlayer spacing behaves in the same way as the interlayer spacing in the bulk. Due to the large number of measured $I(E)$ spectra, the resulting temperature dependence of the interlayer spacing is obviously not caused by statistical errors. The similarity between the bulk expansion coefficient taken from the literature (24×10^{-6} K^{-1}) and the present result (32×10^{-6} K^{-1}) considering the statistical error, provides a good evidence of the quality of these results.

2. rms displacements normal to the surface

As discussed in Sec. III, the rms vibrational amplitudes in the bulk and in the first two layers normal to the surface are also fitting parameters. Figure 7 shows the values of the temperature dependence for these parameters obtained by the fits. In the lower part of Fig. 7 the rms vibrational amplitude determined for the bulk is plotted together with theoretical[27] and experimental[36] data. The straight line is a fit to the theoretical data which shows that these data are well described by a linear temperature dependence. The experimental data show also a linear temperature dependence and the absolute values are in good agreement, too. This result is the first confirmation of theoretical data in a large range of temperature, since up to now only rms vibrational amplitudes for a few temperatures have been available. The scattering of the experimental data is due mainly to statistical errors of the fit procedure and partly also due to instabilities in the electron beam current.

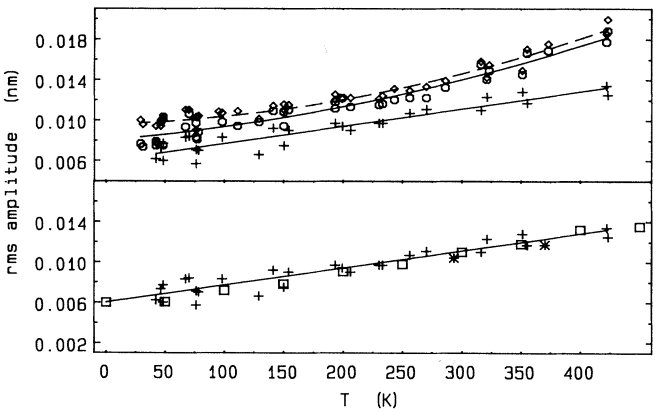

FIG. 7. Temperature dependence of the rms displacements normal to the surface for atoms in the bulk and in the first two layers. In the upper figure the experimental results for the bulk (+ and straight line), the first layer (◇ and dashed line) and the second (○ and solid line) are drawn together with fitted curves to show the tendency of the data. In the lower figure the results for the bulk (+) are shown in comparison to theoretical data (□) (Ref. 27) and to other experimental data (*) (Ref. 36).

In the upper part of Fig. 7 the results are shown for the rms vibrational amplitudes in the two outermost layers together with the rms amplitudes for the bulk. The fitted parabolic lines are traced as a guide to the eyes. The rms amplitudes in the first and second layers are obviously equal within the limits of the experimental errors and show a similar temperature dependence. The rms vibrational amplitudes in the first two layers are larger by about 29% at 300 K and by 38% at 450 K than the corresponding values for the bulk.

3. The inner potential

In all structure determinations using electrons, such as LEED and TEM, the inner potential is an indispensable parameter. In LEED data analysis which is performed by comparison with data calculated within the framework of the dynamical scattering theory, the inner potential is a fit parameter, although it should, in principle, be possible[17] to calculate it with the same atomic potential used in calculation of the phase shifts.

The most direct experimental method for determining V_i is the analysis of the phase shift of the electron waves due to the material by means of an interference microscope.[35,37–39] V_i values for Al obtained by different methods at different electron energies are collected in Table II; they range from 9.3 eV up to 18.2 eV with a mean value of 12.5 eV. The temperature dependence of V_i of Al has not been studied as yet.

In Fig. 8 the $R1$ factor is plotted versus V_i as obtained from the $I(E)$ spectrum measured at $T = 70$ K. The other parameters were fixed at their optimized values in the calculation of the $R1$ factor. The $R1$ factor depends strongly on V_i so that its minimum value of 0.091 is well defined.

The results for V_i are presented in Fig. 9 as a function of temperature where the averaged temperature dependence is shown as a line. In spite of the statistical uncertainties, the data provide clear evidence that the inner potential decreases from about 15 eV at 40 K to 12 eV at 420 K. The observed change of V_i is large in comparison to the temperature dependence of the work function for a metal which is expected to be $-(10^{-4}$–$10^{-5})$ eV/K.[40]

There is only one publication[39] in which the temperature dependence of the inner potential has been described; it is an electron interference microscopy study for Bi. In that case, the inner potential decreases with increasing temperature, too. The decrease depends on

TABLE II. Comparison of various experimental and theoretical results of the inner potential of aluminum. (EIM denotes electron interference microscopy.)

Reference	Method	T (K)	V_i (eV)
Andersen *et al.* (Ref. 1)	LEED	100	9.3
Noonan and Davis (Ref. 2)	LEED	300	10.1
Laramore and Duke (Ref. 53)	LEED	300	16.4
Nielsen and Adams (Ref. 34)	LEED	300	11.6
Hoffman and Jönsson (Ref. 38)	EIM	300	11.9
Buhl (Ref. 35)	EIM	300	12.4
Keller (Ref. 37)	EIM	300	13.0
Keller (Ref. 37)	Theory	0	18.2
Siota (Ref. 52)	Theory	0	9.93

the radius of the examined Bi spheres. The authors assume that this behavior is due to a variation of V_i near the surface. To estimate this temperature dependence of the inner potential, the authors referred to the temperature dependence of the diamagnetic susceptibility which is connected to the inner potential, as reported in Ref. 41 and they found good agreement. Such an estimation is not possible in the case of aluminum because it is paramagnetic.

The inner potentials of both aluminum and bismuth decrease with increasing temperature, but more theoretical and experimental work is necessary to clarify this phenomenon.

C. Corrected peak-shift analysis

As discussed in Sec. III the measured peak shifts (Fig. 3) must be corrected in order to be able to determine the thermal expansion coefficient with respect to the influence of the rms vibrational amplitude [Eq. (4)] and of the inner potential and its temperature dependence [Eq. (2)]. The values of the inner potential shown in Fig. 9 are obtained from the fit described above in addition to the interlayer spacings and rms vibrational amplitudes as already mentioned. As it cannot be excluded that the inner potential depends on the electron energy and shows a different temperature dependence for electrons with lower energies, it is not sure whether the corrected data for the 64-eV peak are valid. In Table III a comparison is made of the thermal expansion coefficients derived from the peaks at 64, 156, and 285 eV with their corrected values.

The correction of the thermal expansion coefficient of 11×10^{-6} K^{-1} derived from the (004) peak using an rms vibrational amplitude of the bulk of 0.105 nm at room temperature[36] and assuming the Debye approximation for the rms vibrational amplitudes leads to a correction of -3×10^{-6} K^{-1}, and the temperature-dependent inner potential gives finally a value of 22×10^{-6} K^{-1}, which due to the relatively large electron penetration depth should correspond to the bulk thermal expansion. Indeed this result is in good agreement with the literature value for the expansion coefficient of the bulk of 24×10^{-6} K^{-1}.[30]

The peak-shift data from the (002) peak at about 64 eV give a corrected value of 48×10^{-6} K^{-1}, which is strongly enhanced compared to the bulk value and the coefficient derived from the analysis of the $I(E)$ spectra. This result should be regarded with caution because of the unknown temperature dependence of the inner potential at that energy, but the data were helpful when looking at the influence of multiple scattering. The strong increase of

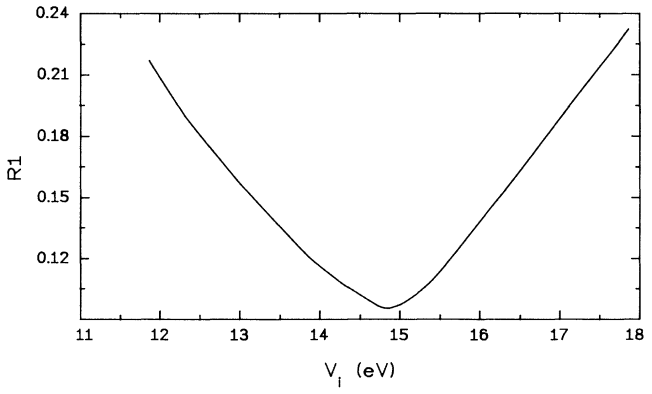

FIG. 8. $R1$ vs V_i calculated for optimum values of the other parameters obtained for an $I(E)$ spectrum taken at 70 K.

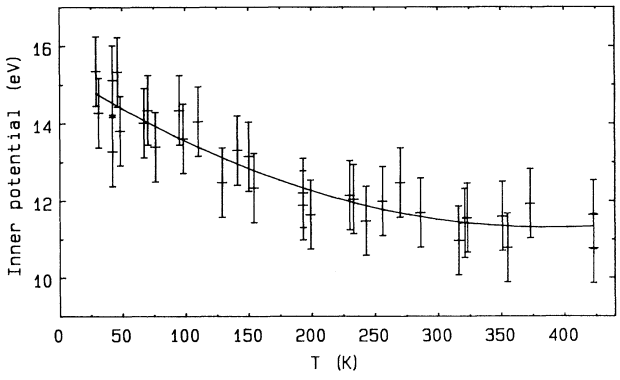

FIG. 9. The temperature dependence of the inner potential of aluminum. The fitted line is just a guide to the eye. The error bars are due to the statistical errors of the fits. The results are derived for the electron energy range from 130 to 420 eV.

TABLE III. Comparison between corrected and uncorrected values of the thermal expansion coefficient α for different electron energies derived for a temperature range from 40 to 450 K.

Peak energy (eV)	α (10^{-6} K^{-1}) uncorrected	α (10^{-6} K^{-1}) corrected
64	21	48
156	12	30
285	11	22

the peak shift above 750 K is correlated to the onset of premelting at that surface as observed with MEIS.[4] The uncorrected value of α is 21×10^{-6} K^{-1} between 40 and 750 K and 64×10^{-6} K^{-1} above 750 K up to 890 K.

The results for the (003) peak at an energy of about 156 eV have been corrected with respect to the known temperature dependence of the inner potential. The corrected value is 30×10^{-6} K^{-1}, with an error that is greater than for the (004) peak, due to the stronger influence of the error of the inner potential.

V. DISCUSSION

No theoretical results are available for the temperature dependence of the interlayer spacings, the thermal expansion coefficient, and the rms vibrational amplitudes at the Al(110) surface. Hence the experimental results are discussed in relation to theoretical work for other fcc (110) surfaces.

The interlayer spacings at the surface and in the bulk were determined by the kinematical analysis of the $I(E)$ spectra for a wide range of temperatures. A comparison is made in Table I between measured and calculated interlayer spacings taken from the literature and typical fit results of this work. The references are sorted chronologically starting with the earliest publication in 1983. All theoretical calculations except those in Ref. 42 yield a damped down oscillating relaxation. To get an overview of the results of the theoretical calculations, it is recommended to look at the range of the first two interlayer spacings: The values of Δd_{12} range from -5.4% to -10.5% and of Δd_{23} range from 1% to 4.8%. These theoretical results do not agree well. The reason for the scattering of the theoretical data has not yet been analyzed, and these model calculations do not consider any temperature dependent effects. Also the origin of the different signs for Δd_{34} obtained in the experimental studies based on the dynamical theory data analysis is not known.

The present results obtained at 70 K show a good agreement with the results from first-principles calculations made by Ho and Bohnen;[43] only the values of Δd_{23} and Δd_{34} are slightly higher. The larger deviation of Δd_{34} from the theoretical results could be due to a greater error regarding the deeper interlayer spacings because the sensitivity of the method decreases with increasing depth. The results obtained at 316 K deviate by a greater amount from the results proposed by Ho and Bohnen, but this could be due to the neglect of temperature dependency in the model calculations. Qualitatively, our results agree with the results of Anderson *et al.*[1]

Analyzing the temperature dependence of the interlayer spacings for the bulk we get a thermal expansion coefficient for the bulk of 32×10^{-6} K^{-1}. This is by about 30% higher than the literature value of 24×10^{-6} K^{-1}. If we assume a statistical error of about 10–15%, the estimated maximum systematical error is about 25%. This large error is due mainly to the very small increase of the lattice constant in that temperature range and the relatively weak sensitivity to the bulk behavior of this method because of the small penetration depth of the electrons.

For the first interlayer spacing we found an increasing contraction with increasing temperature which gives a linear thermal expansion coefficient α_{12} of -24×10^{-6} K^{-1}. This sign of α_{12} is in contradiction to calculations according to a quasiharmonic method proposed by Jayanthi, Tosatti, and Fasolino[44] for the copper (110) surface. For temperatures of less than $0.7T_m$ they found a thermal expansion coefficient for the first interlayer spacing which is of the same magnitude as the bulk value, and for increasing temperature, $T > 0.7T_m$, an enhancement of α_{12} compared to the bulk. Other calculations using MD simulations[14] for the same surface in which the embedded-atom theory was used showed a small contraction of d_{12} of -13.7% to -14.0% in the temperature range from 0 K up to $0.4T_m$. At $T > 0.4-0.5T_m$ thermal expansion at the surface begins to increase. The small contraction of d_{12} with increasing temperature between 0 K and $0.4T_m$ corresponds qualitatively to the contraction found for Al(110) considering that the measurements were made up to $T = 450$ K $\approx 0.5T_m$ (T_m=933.6 K). To prove the theory it is necessary to make specific calculations of the temperature dependence of the mulitlayer relaxation of Al(110).

The data in Fig. 3(a) of the (002) peak are strongly influenced by surface effects because at this energy the mean free path λ is only about 0.5 nm.[25] The layer (i.e., $N_\perp$), which contributes to the scattering, is in this case about 0.3 nm thick; consequently, the derived linear expansion coefficient depends mainly on the expansion of the first two interlayer spacings. For this reason the strong decrease of $\ln[E/E(0)]$ above 750 K ($T > 0.8T_m$) is due to a surface effect. This increase of α is correlated to the onset of premelting on that surface as shown by other experiments[3–5] and theoretical studies.[6–8] In molecular-dynamics simulations it is shown compared with experimental MEIS data[5] that above 750 K the occupied fraction of a top layer decreases and the occupied fraction of the adatom layer increases, starting at zero. The appearance of adatoms is strongly correlated with the onset of disorder at the surface. Other MD calculations[6] predict the melting of the first three layers 200 K below the melting point at about 730 K. Thus the increase of α at 750 K is an indication of the onset of disorder and premelting at the surface. The enhanced interlayer spacing may be a precondition of premelting.

The penetration depth of 285 eV electrons is about two times bigger than that of 64 eV electrons so the surface sensitivity of the former is weaker and the value derived for α (22×10^{-6} K^{-1}) corresponds to the value for the

bulk.[30]

For the second interlayer spacing d_{23} we have determined an expansion coefficient of 55×10^{-6} K^{-1}. This apparently seems to be in contradiction to the discussion above, but for comparison with the peak shift results the mean value of the first three interlayer spacings must be taken which leads to a mean α of about 22×10^{-6} K^{-1} corresponding to the bulk value. This is in good agreement with the results found for Ni(001) (Ref. 12) and Pb(110),[13] too.

The third interlayer spacing gives an α of about 32×10^{-6} K^{-1}, which within the errors band is the same as the bulk value.

A lot of calculations have been made about the onset of premelting at the Al(110) surface,[5–8] but they have not revealed results concerning the temperature dependence of relaxation.

Other experimental results of the thermal expansion of the following surfaces: W(001),[11] Ni(001),[12] and Pb(110),[13] showed also an enhanced expansion compared to the bulk at temperatures higher than 0.5–$0.7T_m$. These expansion coefficients are mean values of the first two or three interlayer spacings depending on the used experimental method.

The contraction of the first interlayer spacing in the low-temperature range can be illustrated by a force model described by Ditlevsen and Nørskov for Al(110):[45] To reduce the corrugation of a (110) surface a contraction of the first interlayer spacing and an expansion of the second interlayer spacing are necessary. The authors give an explanation of the contraction by model calculations based on the effective medium theory using force constants. They found that the force constant between the first and the second layer is greater than the constants between the other layers beneath. The temperature dependence of the force constants may cause an increase in the ratio of the constants between the first and the second layer and the bulk. An increasing ratio for increasing temperature would cause a contraction of d_{12} and a negative expansion coefficient.

Such an effect could be visualized by considering the different interatomic interactions between the interlayers at the surface. Neither the atoms in the first nor the second layer have nearest neighbors in a direction normal to the surface. If we assume that the anharmonicity of the interaction of atoms normal to the surface in the second layer is greater than that of atoms in the the first layer, an increasing temperature would lead to an increasing contraction of d_{12} and a negative expansion coefficient. Except for the errors and fluctuations in the data the rms vibrational amplitude in the first layer normal to the surface is of the same magnitude as in the second layer (Fig. 7). This result supports the thesis that the anharmonicities of the potential in the first and second layer should be similar. The data from measurements made with MEIS on Pb(110) (Ref. 13) and on Al(110) (Ref. 4) can be described with an enhancement of the rms vibrational amplitude normal to the surface amounting to 50% in the first and 25% in the second layer, related to the bulk. These MEIS results are also different from the results of MD simulations obtained by Barnett and Landman[14] for Cu(110). The authors found that below 1000 K the rms vibrational amplitudes in the first layer are smaller than those in the second. On the other hand, the present results are in good agreement with MD calculations made by Yang and Rahman.[46] These authors derived a similar enhancement by about 45% of the rms vibrational amplitude in the first two layers compared to the bulk at $T = 150$ K. But at temperatures above 300 K the rms vibrational amplitudes in the second layer are also greater than in the first layer, the enhancement amounting to 58% compared to the bulk. Thus the rms vibrational amplitudes derived in the kinematical analysis for Al(110) show an enhancement similar to the results of the MD calculations for Cu(110),[46] which is also in good agreement with MD calculations for Ni(110).[15] Whereas the rms vibrational amplitudes for bulk atoms are nearly proportional to the temperature, which is in agreement with the prediction by the microscopic theory,[27] the amplitudes in the first two layers increase more than linearly with the temperature.

Finally, let us ask if one can set some criteria on the applicability of kinematical LEED data analysis. In a series of previous LEED studies[9–12,19–23] the diffraction data have been analyzed in the framework of the kinematical theory. It seems to be astonishing that the energy-dependent data taken for the analysis of steps can be evaluated under neglection of multiple scattering.[21–23] On the other hand, the dynamical theory has to be used for the description of diffraction data if the primary extinction, depending on the value of the scattering amplitude and on the perfection of the sample crystal, dominates the beam attenuation.[47]

The electron mean free path used in our analysis is determined by inelastic processes only.[25,26] Since the experimental $I(E)$ spectra are well described by the calculated kinematical spectra using these data, we may assume that the primary extinction and hence also the multiple scattering are negligible for the selected scattering geometry. But this good agreement holds only for incident angles smaller than a certain critical angle. For greater incident angles additional structures, not reproducible using the kinematical theory, were observed. This may be due to the strong enhancement of the scattering amplitude $f(E,\theta)$ in the forward direction.[18] Such an effect could be explained qualitatively in a simplified picture as follows.

Let us consider a surface layer whose thickness is given by the electron penetration depth. For small incident angles the forward-scattering cone of waves emanating, for example, from an atom in the first layer does not meet atoms outside the row of atoms underneath. For the atoms in the cone, approximated as point scatterers, the scattering geometry is the same for the primary wave and, for instance, a secondary scattered wave, so that single and multiple scattering is indistinguishable. However, for sufficient large incident angles atoms in neighboring rows will be met and multiple scattering with different scattering geometry becomes probable. As a matter of fact, the step-analysis experiments mentioned above were performed at small incident angles.

It should be mentioned that the peak shift test applied

to prove the role of multiple scattering is obviously not as sensitive as the comparison of measured and calculated $I(E)$ spectra. In the former case the peak position measured at larger angles may not be affected unless measured Bragg peak positions due to single scattering are strongly falsified by additional intensity due to multiple scattering.

In summary, the dominating forward scattering in LEED experiments does not cause significant multiple scattering if the incidence angle is small enough. The limit for the angle depends on the aperture of the forward-scattering cone, variable with the electron energy and sample material, on the lattice structure at the surface and on the azimuth angle. If the incident angle is above this limit, the probability for multiple scattering increases with increasing angle.

The kinematical analysis is restricted at high temperature by the decrease of the Debye-Waller factor and the increase of the diffuse background with increasing temperature.

VI. SUMMARY AND CONCLUSION

The method of kinematical LEED data analysis was applied for the determination of the temperature dependence of interlayer spacings and rms vibrational amplitudes in a model study on the Al(110) surface. By the peak-shift method the role of multiple scattering was elucidated with the result that it can be neglected. This observation is in line with results obtained for other surfaces described in the literature. The applicability of the kinematical analysis can be understood by assuming that the electron mean-free-path results mainly from inelastic processes and not from elastic scattering for an appropriately selected incident angle.

The temperature dependences of interlayer spacings and rms vibrational amplitudes normal to the surface are discussed with reference to theoretical results obtained recently for other surfaces described in the literature. The main feature of the low-temperature range, i.e., a negative value of α for the first interlayer spacing and the nearly equally enhanced mean vibrational amplitudes in the first two surface layers, are in accordance with MD results for Cu(110) and Ni(110). Similar MD calculations for Al(110) and model calculations and experiments relating to the inner potentials and their temperature dependence are required. In this work a thermal expansion coefficient enhanced by the factor 2 was detected for $T/T_m > 0.8$, which is in agreement with the results of premelting studies for other surfaces.

[1] J.N. Andersen, H.B. Nielsen, L. Petersen, and D.L. Adams, J. Phys. C **17**, 173 (1984).
[2] J.R. Noonan and H.L. Davis, Phys. Rev. B **29**, 4349 (1984).
[3] P. von Blanckenhagen, W. Schommers, and V. Voegele, J. Vac. Sci. Technol. A **5**, 649 (1987).
[4] A.W. Denier van der Gon, R.J. Smith, J.M. Gay, D.J. O'Connor, and J.F. van der Veen, Surf. Sci. **227**, 143 (1990).
[5] A.W. Denier van der Gon, D. Frenkel, J.W.M. Frenken, R.J. Smith, and P. Stoltze, Surf. Sci. **256**, 385 (1991).
[6] P. Stoltze, N. Nørskov, and U. Landman, Phys. Rev. Lett. **61**, 440 (1988).
[7] P. Stoltze, N. Nørskov, and U. Landman, Surf. Sci. **220**, L693 (1989).
[8] P. Stoltze, J. Chem. Phys. **92**, 6306 (1990).
[9] A. Ignatiev and T.N. Rhodin, Phys. Rev. B **8**, 893 (1973).
[10] U. Romahn, H. Göbel, W. Schommers, and P. von Blanckenhagen, Mod. Phys. Lett. B **5**, 1873 (1991).
[11] J. Kirschner, Phys. Bl. **42** (12), 400 (1986).
[12] Y. Cao and E. Conrad, Phys. Rev. Lett. **65**, 808 (1990).
[13] J.W.M. Frenken, F. Huussen, and J.F. van der Veen, Phys. Rev. Lett. **58**, 401 (1987).
[14] R.N. Barnett and U. Landman, Phys. Rev. B **44**, 3226 (1991).
[15] E.T. Chen, R.N. Barnett, and U. Landman, Phys. Rev. B **41**, 439 (1990).
[16] I.K. Robinson, Phys. Rev. B **33**, 3830 (1986).
[17] M.B. Webb and M.G. Lagally, in *Solid State Physics*, edited by H. Ehrenreich, F. Seitz, and D. Turnbull (Academic, New York, 1973), Vol. 28, p. 301.
[18] M.A. van Hove, W.H. Weinberg, and C.-M. Chan, *Low Energy Electron Diffraction* (Springer-Verlag, Berlin, 1986).
[19] J. Wollschläger, J. Falta, and M. Henzler, Appl. Phys. A **50**, 57 (1990).
[20] A.K. Myers-Beaghton, Surf. Sci. **241**, 439 (1991).
[21] H.-N. Yang, T.-M. Lu, and G.-C. Wang, Phys. Rev. B **43**, 4714 (1991), and references therein.
[22] U. Romahn, P. von Blanckenhagen, C. Kroll, and W. Göpel (unpublished).
[23] W. Weiss, D. Schmeisser, and W. Göpel, Surf. Sci. **207**, 401 (1989).
[24] M.A. van Hove (private communication).
[25] M.P. Seah and W.A. Dench, Surf. Interface Anal. **1**, 1 (1979).
[26] D.R. Penn, Phys. Rev. B **35**, 482 (1987).
[27] E.V. Zarochentsev, S.P. Kravchuk, and T.M. Tarusina, Fiz. Tverd. Tela (Leningrad) **18**, 413 (1976) [Sov. Phys.—Solid State **18**, 239 (1976)].
[28] P.R. Bevington, *Data Reduction and Error Analysis for the Physical Sciences* (McGraw-Hill, New York, 1969).
[29] G. Simmons and H. Wang, *Single Crystal Elastic Constants, A Handbook* (MIT Press, Cambridge, MA, 1971).
[30] *Aluminium*, edited by J.E. Hatch (ASM, Ohio, 1984).
[31] N.M. Butt *et al.*, Acta Crystallogr. Sec. A **44**, 396 (1988).
[32] H. Dosch, T. Höfer, J. Peisl, and R.L. Johnson, Europhys. Lett. **15**, 527 (1991).
[33] H. Göbel, W. Getto, and P.v. Blanckenhagen, Verhandl. DPG (VI)26, O7.7 (1991).
[34] H.B. Nielsen and D.L. Adams, J. Phys. C **15**, 615 (1982).
[35] R. Buhl, Z. Phys. **155**, 395 (1959).
[36] R.E. Dingle and E.H. Medlin, Acta Crystallogr. Sec. A **28**, 22 (1972).
[37] M. Keller, Z. Phys. **164**, 27 (1961).
[38] H. Hoffmann and C. Jönsson, Z. Phys. **182**, 360 (1965).
[39] H. Berger, Yu.A. Kulyupin, S.A. Nepijko, I.A. Obuchov, and V.G. Shamonya, Z. Phys. B **37**, 23 (1980).

[40]J. Hölzl and F.K. Schulte, in *Work Function of Metals*, edited by G. Höhler, Springer Tracts in Modern Physics Vol. 85 (Springer-Verlag, Berlin, 1979).
[41]S. Miyake, Proc. Phys. Soc. Jpn. **22**, 666 (1940).
[42]A.G. Eguiluz, Phys. Rev. B **35**, 5473 (1987).
[43]K.M. Ho and K.P. Bohnen, Phys. Rev. B **32**, 3446 (1985).
[44]C.S. Jayanthi, E. Tosatti, and A. Fasolino, Surf. Sci. **152/153**, 155 (1985).
[45]P.D. Ditlevsen and J.K. Nørskov, Surf. Sci. **254**, 261 (1991).
[46]L. Yang and T.S. Rahman, Phys. Rev. Lett. **67**, 2327 (1991).
[47]R.W. James, in *Solid State Physics*, edited by F. Seitz and D. Turnbull (Academic, New York, 1963), Vol. 15.
[48]J.R. Smith and A. Banerjea, Phys. Rev. B **37**, 10411 (1988).
[49]R.N. Barnett, U. Landman, and C.L. Cleveland, Phys. Rev. B **27**, 6534 (1983).
[50]T. Ning, Q. Yu, and Y. Ye, Surf. Sci. **206**, L857 (1988).
[51]S.P. Chen, A.F. Voter, and D.J. Srolovitz, Phys. Rev. Lett. **57**, 1308 (1986).
[52]Y. Siota, The Science Reports of the Tôhoku University, Vol. XLII, No. 4, 1958 (unpublished).
[53]G.E. Laramore and C.B. Duke, Phys. Rev. B **5**, 267 (1972).